

# Verifying Operational Forecasts of Land-Sea Breeze and Boundary Layer

## Mixing Processes

Ewan Short\*

*School of Earth Sciences, and ARC Centre of Excellence for Climate Extremes, The University of  
Melbourne, Melbourne, Victoria, Australia.*

Ben ?. Price

*Bureau of Meteorology, Casuarina, Northern Territory, Australia*

Derryn ?. Griffiths and Alexei ?. Hider

*Bureau of Meteorology, Melbourne, Victoria, Australia*

\*Corresponding author address: School of Earth Sciences, The University of Melbourne, Melbourne, Victoria, Australia.

E-mail: shorte1@student.unimelb.edu.au

## ABSTRACT

13 This paper presents a method for verifying the diurnally varying compo-  
14 nent of the wind forecasts issued by the Australian Bureau of Meteorology.  
15 These wind forecasts are based on model data that is then edited by human  
16 forecasters. The model datasets most commonly used by Australian forecast-  
17 ers for winds are those of the European Center for Medium-Range Weather  
18 Forecasting (ECMWF) and the Australian Community Climate and Earth Sys-  
19 tem Simulator (ACCESS). The methodology is applied to the coastal weather  
20 stations across Australia over June, July and August 2018, at three different  
21 spatial scales, on both a daily and seasonal basis. The results indicate that  
22 while the Official forecast outperforms unedited ACCESS and ECMWF at  
23 certain locations and times of day, it rarely outperforms both at once. The  
24 causes of the differences in the performance of each dataset vary by location,  
25 but can include biases in the direction at which the sea-breeze approaches the  
26 coast, amplitude biases in the diurnal cycle, and disagreement as to whether  
27 sea-breeze or boundary layer mixing processes contribute most to the diurnal  
28 cycle. Furthermore, when winds are compared at small spatial scales on a  
29 daily basis, ECMWF outperforms Official and ACCESS simply because its  
30 coarser resolution creates less internal variability than Official or ACCESS.  
31 These results have implications for forecasting practice, verification method-  
32 ology, and the way forecasts are interpreted and communicated.

## 33 1. Introduction

34 Modern weather forecasts are typically produced by models in conjunction with human forecast-  
35 ers. Forecasters working for the Australian Bureau of Meteorology construct a seven day forecast  
36 by first loading model data into a software package called the Graphical Forecast Editor (GFE),  
37 then editing this model data using tools within GFE. Is this also how things work at the U.S Na-  
38 tional Weather Service and U.K. Met Office? Forecasters can choose which model to base their  
39 forecast on, and refer to this as a choice of *model guidance*. Edits are typically made to account for  
40 processes that are under-resolved at synoptic scale model resolutions, or to address known biases  
41 of the models being used.

42 Australian forecasters typically make two kinds of routine daily edits to the surface wind fields.  
43 Two edits are commonly involves changing the surface wind fields near coastlines to try to rep-  
44 resent sea-breezes more realistically. Forecasters invest time in making sea-breeze edits because  
45 accurate predictions of near-surface winds are highly valued by a number of users, such as the  
46 aviation and energy (Smith et al. 2009) industries. Accurate sea-breeze forecasts are also valuable  
47 to environmental monitoring authorities, as these winds provide ventilation to coastal urban areas.

48 Assessing the accuracy of a weather forecast is a task far more nuanced than it might first appear.  
49 For instance, attempting to assess the accuracy of a precipitation forecast by comparing the rainfall  
50 amounts measured at an individual weather station to the closest grid point of a model prediction  
51 will often give poor results. Although the synoptic drivers of convection are usually well predicted,  
52 exactly where convective cells form, and where the most rain falls, is highly unpredictable. As  
53 such, it is often appropriate to use “fuzzy” verification metrics which measure the agreement  
54 between prediction and observation in a more indirect way. For instance, one approach known as  
55 “upscaling” is to first average forecast and observational data over a given spatial domain before

56 calculating verification scores. Ebert (2008) provided a review of current “fuzzy verification”  
57 methodologies, and a framework for how they can be used to determine the spatial scales at which  
58 a given forecast has predictive skill.

59 Relatively few forecast verification studies have focused on near-surface winds, and the ones  
60 that have generally only considered wind speeds. Pinson and Hagedorn (2012) performed a veri-  
61 fication study of the ECMWF 10 m wind speeds across western Europe over December, January,  
62 February 2008/09. First, they interpolated ECMWF model data onto the locations of weather  
63 stations across Europe, then they compared the interpolated model data at these stations with the  
64 station observations themselves. They found that the worst performing regions were coastal and  
65 mountainous areas, and attributed this poor performance to the small scale processes, e.g. sea  
66 and mountain breezes, that are underresolved at ECMWF’s coarse 50km spatial resolution. They  
67 noted that future work could better identify the effect of diurnal cycles on verification statistics by  
68 considering forecasts at different times of day.

69 Lynch et al. (2014) also performed a verification study of ECMWF 10 m wind speed data, with  
70 the goal of assessing skill at lead times of between 14 to 20 days. They compared ECMWF 32-  
71 day forecast model wind speeds with gridded ERA-Interim wind speeds between 2008-12, with  
72 both datasets analysed at a six hour temporal resolution. Before conducting the comparison, the  
73 wind speed data were transformed into wind-speed “anomaly” data by first calculating the mean  
74 wind speed at 0000, 0600, 1200 and 1800 UTC for each calendar day from the entire ERA-Interim  
75 record, and from a 20 year ECMWF 32-day model hindcast, then subtracting these means from the  
76 ERA-Interim and ECMWF 32-day model data respectively. Wind speed anomaly data was used  
77 so that stable seasonal and diurnal cycles did not contribute to verification scores. At the 14-20  
78 day timescale around western Europe, the greatest skill was found in the boreal winter (austral  
79 summer) months of December, January and February.

80 Pinson and Hagedorn (2012) and Lynch et al. (2014) restricted their verification studies to wind  
81 speeds, but wind directions are also crucial to diagnosing whether land sea breezes - and the diurnal  
82 wind cycle more generally - are being forecast correctly. Furthermore, no previous published  
83 work has proposed a verification methodology to assess the accuracy of the diurnal wind cycle  
84 in forecasts, or of the contributions made to this accuracy by human forecaster edits of model  
85 output. Finally, no previously published work has considered the performance of ACCESS near  
86 surface winds, which together with ECMWF, are the model guidance products most widely used  
87 by Australian forecasters. Thus, the present study has two goals. First, to describe a methodology  
88 for comparing human edited forecasts of the land-sea breeze to unedited model guidance forecasts,  
89 in order to assess where and when human edits are producing an increase in accuracy. Second,  
90 to apply this methodology across Australia. The remainder of this paper is organised as follows.  
91 Section 2 describes the methodology in detail, section 3 provides results, and sections 4 and 5  
92 provide a discussion and a conclusion, respectively.

## 93 **2. Data and Methods**

94 This study compares both edited and non-edited Australian Bureau of Meteorology forecast  
95 data with automatic weather station (AWS) data across Australia. The comparison is performed  
96 by first isolating the diurnal signals of each dataset, then comparing these signals on an hour-by-  
97 hour basis. If the diurnal cycle cannot be resolved correctly using wind perturbations, it cannot be  
98 resolved correctly in the overall wind fields, which are subject to additional synoptic scale errors  
99 between the models and observations.

## 100 *a. Data*

101 Four datasets are considered in this study; they are the Australian Bureau of Meteorology's Of-  
102 ficial wind forecast data, model data from the European Center for Medium Range Weather Fore-  
103 casting (ECMWF), model data from the Australian Community Climate and Earth System Simu-  
104 lator (ACCESS), and observational data from automatic weather stations. The Official, ECMWF  
105 and ACCESS data are at a ?, ? degree spatial resolution respectively. What are the resolutions of  
106 these datasets as they're used in Jive? Does the ACCESS model data in Jive Official, ACCESS  
107 and AWS data exists at each UTC hour. ECMWF data exists at a three hour resolution. To be con-  
108 sistent with the other data sets, ECMWF is therefore linearly interpolated to an hourly resolution:  
109 this is also what happens in practice when forecasters load ECMWF wind data into the GFE. Both  
110 ACCESS and ECMWF use parametrisation schemes to simulate sub-grid scale boundary layer  
111 mixing and turbulence. ACCESS uses the schemes of Lock et al. (2000) and Louis (1979) for  
112 unstable and stable boundary layers respectively (Bureau of Meteorology 2010). ECMWF uses  
113 similar schemes that they develop in-house (European Center for Medium Range Weather Fore-  
114 casting 2018). Data covers the austral winter months of June, July and August 2018; this short  
115 time period was chosen to reduce the effect of changing seasonal and climatic conditions, changing  
116 forecasting practice and staff, and of developments to the ACCESS and ECMWF models.

117 How is model/forecast data made consistent with AWS data in Jive - particularly regarding  
118 heights? Are all stations 10 m above surface? Are all model/forecast data provided at the same  
119 height?

120 Only station data from the seven Australian capital city airport automatic weather stations are  
121 considered; Official, ECMWF and ACCESS data is (linearly?) interpolated to the coordinates  
122 of the airport weather stations. Capital city airports have been chosen as the focus of this study

123 for a number of reasons. Automatic weather stations located at airports tend to provide the most  
124 accurate wind data, and wind forecasts at airports are important to the aviation industry. Moreover,  
125 the capital city airports are all reasonably close to coastlines, resulting in a clear diurnal signal.  
126 Finally, these airports are also all close to their respective capital cities, which are high priority  
127 regions for accurate forecasting. The datasets are hosted on the Bureau's Jive database, but are not  
128 currently generally available, although the long term plan is for this to change. **Can I extract and**  
129 **host the data I need myself? Can I obtain copies of the relevant Jive Functions so that I can post**  
130 **complete code online?**

131 As described above, the Australian Bureau of Meteorology's official wind forecast is constructed  
132 out of model data, which is then edited by human forecasters using the Graphical Forecast Editor  
133 (GFE) software package. Australian forecasters typically construct wind forecasts out of model  
134 data either from the European Center for Medium Range Weather Forecasting (ECMWF), or the  
135 Australian Community Climate and Earth System Simulator (ACCESS). Testing whether the of-  
136 ficial forecast data conforms more closely to the AWS observations than ECMWF or ACCESS  
137 therefore provides a way to assess the extra accuracy gained by forecaster edits.

### 138 *b. Assessing Diurnal Cycles*

139 Although close to coastlines the land-sea breeze is generally the dominant diurnal wind process,  
140 the overall diurnal signal may also include mountain-valley breezes, boundary layer mixing pro-  
141 cesses, atmospheric tides, and urban heat island circulations. Forecasters typically edit model out-  
142 put to account for *both* unresolved sea-breezes *and* unresolved boundary layer mixing; attempting  
143 to focus solely on sea-breezes without examining the entire diurnal cycle therefore risks erroneous  
144 conclusions, with the effects of one category of edit mistaken for another. **In general it is hard to**

separate boundary layer mixing edits from sea-breeze edits in the diurnal cycle composites, so this point maybe needs to be reworked. Or could simply comment on this in the discussion.

Sea-breezes are therefore analysed by examining the overall diurnal signal in each dataset, with the assumption that close to coastlines the land-sea breeze is the dominant diurnal process. The diurnal signal is identified by subtracting a twenty hour centred running mean *background wind* from each zonal and meridional hourly wind data point. This provides a collection of zonal and meridional wind *perturbation* datasets. Note that thinking of land-sea breezes in terms of perturbations from a background wind may require a conceptual shift from the usual operational definitions. A forecaster would likely define a sea-breeze to be a reversal in wind direction from a primarily offshore flow during the night and morning, to an onshore flow in the afternoon and evening. However, even if the wind is offshore the entire day, sea-breeze *perturbations* are generally still detectable as a weakening of the offshore flow throughout the afternoon and evening.

Note that subtracting background winds may raise concerns, because perturbations obviously depend on background winds. However, the forecaster does not have knowledge of the observations when they make the diurnal process edits. They are implicitly assuming that the true mean state will be close enough to the predicted mean state - however this prediction is produced - to justify making diurnal edits on the basis of the predicted mean state.

Once the wind perturbation datasets have been constructed, the accuracy of the Official, ACCESS and ECMWF diurnal cycles are quantified by first calculating the Euclidean distances of the perturbations at each hour from the corresponding AWS perturbations. For instance, to quantify how closely the Official forecast perturbations match the AWS observations, we calculate the Euclidean distances  $|u_{\text{AWS}} - u_{\text{O}}|$  at each time step. The accuracy with which the Official and ACCESS datasets resolve the diurnal cycle can then be compared by defining the *Wind Perturbation*



## Index (WPI)

$$\text{WPI}_{\text{OA}} \equiv |\mathbf{u}_{\text{AWS}} - \mathbf{u}_{\text{A}}| - |\mathbf{u}_{\text{AWS}} - \mathbf{u}_{\text{O}}|. \quad (1)$$

At a given time, the Official forecast wind perturbation is closer to the AWS perturbation than that of ACCESS if and only if  $\text{WPI} > 0$ . Similarly, the WPI can be used to provide a comparison of the Official and ECMWF datasets, or a comparison of the two model guidance datasets ACCESS and ECMWF.

To assess which dataset provides, in general, the most accurate representation of the diurnal cycle, we then take means of the WPI on an hourly basis; i.e. all the 00:00 UTC WPI values are averaged, all the 01:00 UTC values are averaged, and so forth. The sampling distributions of these means can then be modelled as Student's  $t$ -distributions, and from this we can calculate the probability that  $\overline{\text{WPI}} > 0$  at each hour, where the bar denotes a temporal average. Temporal autocorrelations of WPI, i.e. correlations between WPI values at a particular hour from one day to the next, are accounted for using the standard method of reducing the “effective” sample size to  $n(1 - \rho_1)/(1 + \rho_1)$ , where  $n$  is the actual sample size and  $\rho_1$  is the lag-1 autocorrelation (Zwiers and von Storch 1995; Wilks 2011), although in practice temporal autocorrelations of WPI are either non-existent or very small. To assess how well the diurnal perturbations of an overall region are predicted, for instance those of the Victorian coastal station group (see Fig. ??), the perturbations across each station group are averaged before WPI values are calculated. The temporal means and sampling distributions of the WPI are then calculated as before, with each value of WPI calculated from the spatially averaged perturbations treated as a single observation. This provides a conservative method for dealing with spatial correlation in the perturbations.

The advantage of the WPI method is its clarity and simplicity: we are essentially just comparing the magnitudes of vector differences, then applying a two-sided  $t$ -test to determine whether one dataset's perturbations are consistently closer to observations than another's. One factor that com-

191 plicates interpretation of statistics of WPI, is that the near surface winds observed in AWS data are  
 192 consistently noisier than those of the Official, ECMWF and ACCESS forecasts. This is likely due  
 193 to unresolved subgrid scale turbulence in the Official, ECMWF and ACCESS model datasets. It  
 194 would be unreasonable to expect forecasters to be able to predict this essentially random additional  
 195 observed variability, and so a direct comparison of observed and modelled diurnal cycles is overly  
 196 stringent.

197 To reduce the significance of unpredictable noise, we also compare temporal averages of the  
 198 perturbations for each dataset. These comparisons have less operational significance: people gen-  
 199 erally care how well the actual weather forecast performed, not whether the average of a predicted  
 200 quantity matched the average of an observed quantity. However, comparisons of averages arguably  
 201 better represent what we can realistically expect from human forecaster edits, and from weather  
 202 forecasts overall, particularly in regards to small scale processes like sea-breezes. Furthermore,  
 203 when temporal averages of perturbations are considered, the diurnal signal becomes dramatically  
 204 clearer, and structural differences become much easier to diagnose.

205 To quantify how closely the temporally averaged Official forecast perturbations match those of  
 206 the AWS observations, we calculate  $|\bar{\mathbf{u}}_{\text{AWS}} - \bar{\mathbf{u}}_{\text{O}}|$  for each hour. To assess the performance of the  
 207 Official temporally averaged perturbations against those ACCESS, we define the *Climatological*  
 208 *Wind Perturbation Index* (CWPI)

$$\text{CWPI}_{\text{OA}} \equiv |\bar{\mathbf{u}}_{\text{AWS}} - \bar{\mathbf{u}}_{\text{O}}| - |\bar{\mathbf{u}}_{\text{AWS}} - \bar{\mathbf{u}}_{\text{A}}|. \quad (2)$$

209 As with the WPI, the CWPI can also be used to provide a comparison of the Official and ECMWF  
 210 datasets, or a comparison of the two model guidance datasets ACCESS and ECMWF. Uncertainty  
 211 in the CWPI is estimated through bootstrapping (Efron 1979). This is done by performing resam-  
 212 pling with replacement on the underlying perturbation datasets, and calculating the CWPI multiple

times using these resampled datasets. This provides a distribution of CWPI values, from which the probability that  $CWPI > 0$  can be calculated. Similarly to with the WPI, performance over a particular region can be assessed by first averaging perturbation values over multiple stations before the CWPI is calculated.

Although the WPI and CWPI provide quantitative information on the accuracy of the diurnal cycle at different times of day, they do not provide much information about the structure of the diurnal wind cycles of each dataset, or provide insight into the reason one dataset is outperforming another. Gille et al. (2005) obtained summary statistics on the observed structure of temporally averaged diurnal wind cycles across the globe by using linear regression to calculate the coefficients  $u_i$ ,  $v_i$   $i = 0, 1, 2$ , for the elliptical fit

$$u = u_0 + u_1 \cos(\omega t) + u_2 \sin(\omega t), \quad (3)$$

$$v = v_0 + v_1 \sin(\omega t) + v_2 \cos(\omega t), \quad (4)$$

where  $\omega$  is the angular frequency of the earth and  $t$  is the local solar time in seconds. Descriptive quantities - like the angle the semimajor axis of the ellipse makes with the horizontal - were then calculated directly from the coefficients  $u_1$ ,  $u_2$ ,  $v_1$  and  $v_2$ .

Gille et al. (2005) applied this fit to satellite scatterometer wind observations, which after temporal averaging provided only four temporal datapoints at each  $0.25^\circ \times 0.25^\circ$  spatial grid cell. As such, their fit was very good, explaining over 90% of the wind variability in each spatial gridcell. However, the choice of ellipse parametrisation in equations 5 and 6 assumes that datapoints lie on the ellipse at equal intervals of time  $t$ . When observational or model data with an hourly or smaller timestep is considered, this assumption becomes too stringent, as heating asymmetries imply that wind perturbations evolve much more rapidly during the day than at night (see Fig. XX). **Note**

I'm also basing this point on knowledge of the land vs sea breeze, and knowledge of heating vs cooling asymmetries (Brown et al. 2017, e.g.).

Thus, we model the climatological diurnal cycles with the equations

$$u = u_0 + u_1 \cos(\alpha(\psi, t)) + u_2 \sin(\alpha(\psi, t)), \quad (5)$$

$$v = v_0 + v_1 \sin(\alpha(\psi, t)) + v_2 \cos(\alpha(\psi, t)), \quad (6)$$

with  $\alpha$  the function from  $[0, 24) \times [0, 2\pi) \rightarrow [0, 2\pi)$  given by

$$\alpha(\psi, t) \equiv \pi \left[ \sin \left( \pi \frac{(t - \psi) \bmod 24}{24} - \frac{\pi}{2} \right) + 1 \right], \quad (7)$$

where  $t$  is time in units of hours UTC, and  $\psi$  gives to the time when the wind perturbations vary least with time. **Need to confirm whether least or most!** For each climatological diurnal wind cycle, we solve for the seven parameters  $u_0, u_1, u_2, v_0, v_1, v_2$  and  $\psi$  using nonlinear regression.

Descriptive quantities can then be calculated from these parameters. The value of  $\alpha$  at which the winds align with the semimajor axis,  $\alpha_M$ , satisfies

$$\alpha_M = \frac{1}{2} \arctan \left( \frac{2(u_1 u_2 + v_1 v_2)}{u_1^2 + v_1^2 - u_2^2 - v_2^2} \right) \bmod \pi, \quad (8)$$

The time at which the perturbations align with the major axis  $t_M$  can then be calculated by inverting equation (7), fixing  $\psi$  to the value obtained from the nonlinear regression. The lengths of the semimajor and semiminor axes, and the angle the semimajor axis makes with lines of latitude  $\phi$ , can then be calculated from  $\alpha_M$  using the same expressions as Gille et al. (2005).

### 3. Results

In this section, the methods described in section ?? are applied to Australian forecast and station data over the months of June, July and August (austral winter) 2018. First, error is assessed on a daily basis using the Wind Perturbation Index (WPI) at three different spatial scales. Second,

250 overall seasonal biases during this time period are assessed using the Climatological Wind Pertur-  
251 bation Index CWPI, and by comparing quantities derived from ellipses fitted to the climatological  
252 wind perturbations. Unless otherwise stated, values throughout this section are provided to two  
253 significant figures.

#### 254 *a. Daily Comparison*

255 Figure 2 provides the mean wind perturbation index values  $\overline{wpi}$  and confidence scores  
256  $P(\overline{WPI} > 0)$  for the coastal station groups for  $\overline{wpi}_{OA}$ ,  $\overline{wpi}_{OE}$  and  $\overline{wpi}_{EA}$ , which represent the the  
257 Official versus ACCESS, Official versus ECMWF, and ECMWF versus ACCESS comparisons,  
258 respectively. Values of  $\overline{wpi}_{OA}$  and  $\overline{wpi}_{OE}$  are negative for the majority of station groups and hours,  
259 and often both  $P(\overline{WPI}_{OA} > 0) < 5\%$  and  $P(\overline{WPI}_{OE} > 0) < 5\%$ . This implies that at this level of  
260 spatial aggregation, there is often high confidence that both the unedited ACCESS and ECMWF  
261 models outperform the Official forecast. The lowest  $\overline{wpi}$  values of  $-0.9$  kn occur for the NT sta-  
262 tion group at 23:00 and 00:00 UTC for both  $\overline{wpi}_{OA}$  and  $\overline{wpi}_{OE}$ , with  $\overline{wpi}_{EA} = 0$  kn. Comparatively  
263 low values also occur at 08:00 UTC with  $\overline{wpi}_{OA} = \overline{wpi}_{OE} = -0.6$  kn, but  $\overline{wpi}_{EA} = 0$  kn. This  
264 suggests the Official forecast may be performing particularly poorly over the NT station group.

265 Although Official outperforms at least one of ACCESS or ECMWF with high confidence at  
266 a few dozen times and station groups, there is only one group and time where it outperforms  
267 both. At 05:00 UTC over the South WA station group,  $\overline{wpi}_{OA} = 0.2$  kn and  $\overline{wpi}_{OE} = 0.1$  kn, both  
268 with confidence scores  $\geq 95\%$ , although the actual  $\overline{wpi}$  values are comparatively small. Note that  
269 ECMWF generally outperforms ACCESS from 10:00 - 14:00 UTC, with the South WA station  
270 group being the main exception.

271 Using the NT and South WA station groups as case studies, Figures 3 a) and b) provide time  
272 series of  $wpi_{OA}$  and  $wpi_{OE}$  for, a), the NT station group at 23:00 UTC, and b), the South WA

station group at 05:00 UTC. The  $wpi_{OA}$  and  $wpi_{OE}$  values for the NT station group show significant temporal variability over the three month period, exceeding  $-2$  kn on at least 10 days each, and occasionally becoming positive. The  $wpi$  values for the South WA station at 05:00 UTC also show significant temporal variability, with  $wpi_{OA}$  and  $wpi_{OE}$  each exceeding 1 kn on at least 9 separate days, despite  $\overline{wpi}_{OA}$  and  $\overline{wpi}_{OE}$  being small.

Fig. 3 a) shows that there are four days where  $wpi_{OA}$  and  $wpi_{OE}$  are both less than  $-2$  kn: the 8<sup>th</sup> of June and the 3<sup>rd</sup>, 9<sup>th</sup> and 10<sup>th</sup> of July. Figures 3 c) and d) show hodographs of the winds and wind perturbations, respectively, at each hour UTC for the AWS observations, Official forecast, and ACCESS and ECMWF model datasets on the 3<sup>rd</sup> of July, which provides an interesting example. Figure 3 e) shows that the Official wind forecast on this day was likely based on edited ACCESS from 00:00 to 06:00 UTC, then edited ECMWF from 07:00 to 13:00 UTC, then unedited ACCESS from 15:00 to 21:00 UTC. The final two hours of the forecast show the Official winds acquiring a stronger east-northeasterly component than either the AWS observations, ACCESS, or ECMWF; this rapid, exaggerated change is even clearer in the perturbation hodograph shown in Fig. 3 f). Note that at this time of year the prevailing winds throughout the NT are east-southeasterly, and 22:00 UTC corresponds to  $\approx 08:30$  LST in this region, so the rapid departure of the Official forecast from ACCESS at this time likely represents an edit made by a forecaster to capture boundary layer mixing processes. Figure 4 a) shows the first ten values from wind soundings at Darwin Airport - the nearest station to issue vertical wind soundings - at 12:00 UTC on July 3<sup>rd</sup> and 00:00 UTC on July 4<sup>th</sup>. In both instances the winds are indeed east-southeasterly, and so the rapidly changing wind perturbations at 22:00 UTC in the Official forecast likely reflect a boundary layer mixing edit that has been applied either too early, or has strengthened the south-easterly component of the winds too much. The 8<sup>th</sup> of June and 9<sup>th</sup> and 10<sup>th</sup> of July examples are all similar in this respect.

297 Considering now the South WA station group, Fig. 3 b) shows that  $wpi_{OA}$  and  $wpi_{OE}$  both ex-  
 298 ceed 1 kn on the 9<sup>th</sup> of June and the 3<sup>rd</sup> of August. Figures 3 c) and d) show hodographs of the  
 299 winds and wind perturbations, respectively, at each hour UTC for the AWS observations, Official  
 300 forecast, and ACCESS and ECMWF model datasets on the 9<sup>th</sup> of June, which is the more interest-  
 301 ing example. The perturbation hodograph shows both ECMWF and ACCESS underpredicting the  
 302 amplitude of the diurnal wind cycle on this day. In each dataset the 05:00 UTC perturbations are  
 303 westerly to northwesterly, and given the orientation of the South WA coastline (see Fig. 1) and the  
 304 fact that 05:00 UTC corresponds to  $\approx 13:00$  local solar time (LST) in this region, the perturbations  
 305 likely indicate boundary layer mixing processes, rather than the land-sea breeze. Furthermore, the  
 306 AWS perturbations rapidly become northwesterly between 01:00 and 02:00 UTC,  $\approx 09:00 - 10:00$   
 307 LST, which would be about three hours after the sun has risen, consistent with a boundary layer  
 308 mixing mechanism.

309 Figure 4 provides hodographs of wind with height throughout the first two km of the atmosphere  
 310 between 12:00 UTC on the 8<sup>th</sup> June and 12:00 UTC on the 9<sup>th</sup> June; the soundings were taken at  
 311 Perth Airport, which is the nearest station to the South WA station group to provide wind sound-  
 312 ings. The 8<sup>th</sup> June 12:00 UTC hodograph shows surface northerlies of  $\approx 6$  kn, becoming west to  
 313 northwesterlies of over 20 kn 2.4 km above the surface. A forecaster basing a model edit of the  
 314 following days winds on this sounding would therefore gradually strengthen the westerly compo-  
 315 nent of the surface winds in the hours after sunrise. However, the subsequent sounding at 00:00  
 316 UTC on the 9<sup>th</sup> of June shows that the winds acquire a strong northerly component of 30 kn in the  
 317 first 500 m of the atmosphere, with the final sounding indicating a strong northwesterly wind at  
 318 725 m persisting until 12:00 UTC. In Fig. 3 d), the Official perturbations from 04:00 to 07:00 UTC  
 319 show stronger westerly perturbations than either ACCESS or ECMWF, improving the amplitude  
 320 of Official's diurnal wind cycle. However, the AWS perturbations are more northerly than those of

Official, and so the Official forecast winds have been strengthened in a slightly incorrect direction. An explanation for this discrepancy is that the Official forecast for the southwest region of WA has been edited based on the June 8<sup>th</sup> 12:00 UTC Perth Airport sounding, with the winds above the surface changing direction in the subsequent 12 hours. Note that the 3<sup>rd</sup> of August example is similar, although in this case the Official forecast slightly improves both the magnitude and direction of the 05:00 UTC wind perturbations.

Figure 5 presents the  $\overline{wpi}$  values and confidence scores for the Official versus ECMWF comparisons, i.e.  $\overline{wpi}_{OE}$  and  $P(\overline{WPI}_{OE} > 0)$ , for the airport stations, and airport station groups. The results for the airport stations are noisier than the analogous results for the coastal station groups in Figures 2 c) and d), although they do share some similarities. Official outperforms ECMWF at 01:00 and 02:00 UTC at both the Darwin airport station and the NT station group, although ECMWF outperforms Official between 08:00 and 14:00 UTC at Darwin and Brisbane airports, and the corresponding NT and QLD station groups, with the exception of the QLD station group at 12:00 UTC where  $\overline{wpi}_{OE} = 0$ . ECMWF also outperforms Official at Hobart airport at almost all hours of the day, and at Adelaide and Canberra airports from 11:00 to 14:00 UTC.

For the remaining stations and times, only the Perth airport station at 06:00 UTC and the Melbourne airport station at 01:00 UTC exhibit  $\overline{wpi}_{OE} > 0$  with  $P(\overline{WPI}_{OE} > 0) \geq 95\%$ . However, in both cases  $\overline{wpi}_{OE} = 0.3$ , which is small compared to the maximum value of 1.0 which occurs at the Darwin airport station at 02:00 UTC. Furthermore, in both cases there is no clear pattern to the  $\overline{wpi}_{OE}$  values over the rest of the day. Given the random appearance of the  $\overline{wpi}_{OE}$  values, the *multiplicity problem* (Wilks 2011, p. 178) requires care be taken before giving meaning to these two examples: i.e., given that we are calculating twenty four confidence scores for eight stations, then assuming WPI were uncorrelated across each station and hour we would expect to



344 find  $0.05 \times 24 \times 8 \approx 10$  instances where  $P(\overline{\text{WPI}}_{\text{OE}} > 0) \geq 95\%$ , even if  $\overline{\text{WPI}}_{\text{OE}}$  was in fact equal  
345 to zero. **Comment on performance versus ACCESS.**

346 For the airport station groups, ECMWF outperforms Official for the majority of station groups  
347 and times. The main exception is the Darwin airport station group, where Official outperforms  
348 ECMWF at 02:00 UTC, and there is ambiguity as to whether Official or ECMWF performs better  
349 at 01:00, 03:00 and 04:00 UTC, and from 15:00 to 22:00 UTC. In the analogous comparisons  
350 of Official and ACCESS (not shown), the airport station results are similarly noisy, although the  
351 airport station group results are slightly more favourable to Official, with Official outperforming  
352 ACCESS from 10:00 to 12:00 UTC at the Brisbane station group, and fewer occasions overall  
353 where ACCESS outperforms Official than ECMWF does.

354 Figure 5 shows the  $\overline{\text{wpi}}$  values and confidence scores for the ECMWF versus ACCESS compar-  
355 isons, i.e.  $\overline{\text{wpi}}_{\text{EA}}$  and  $P(\overline{\text{WPI}}_{\text{EA}} > 0)$ , for the airport stations, and airport station groups. As with  
356 the Official versus ECMWF comparison in Fig. 5, the results for the airport stations are noisy, but  
357 more often than not show that ECMWF outperforms ACCESS. The results for the airport station  
358 group show ECMWF usually outperforms ACCESS, the main exceptions being the Darwin and  
359 Canberra airport station groups.

360 At face value, the fact that ECMWF generally outperforms ACCESS at these scales is surprising,  
361 as ACCESS runs at a higher spatiotemporal resolution than ECMWF, and is calibrated for Aus-  
362 tralian conditions, so one would expect ACCESS would better resolve small scale processes like  
363 the land-sea breeze and boundary layer mixing processes. However, these results are unsurprising  
364 if one considers the scales at which predictable atmospheric motion occurs, and the scales being  
365 resolved by AWS, ACCESS and ECMWF. The AWS data resolves motion with time scales as low  
366 as 10 minutes, and arbitrarily small spatial scales: it therefore includes highly unpredictable eddy  
367 turbulence. This explains why the results for the airport stations are noisier than for the airport sta-

tion groups or coastal station groups. Furthermore, because ACCESS runs at a higher resolution than ECMWF, it includes additional scales of motion, and therefore adds additional variability to the wind fields. Unless this additional variability in ACCESS is perfectly correlated with observations, the average of  $|\mathbf{u}_{\text{AWS}} - \mathbf{u}_A|$  will therefore increase, unless this additional variability is compensated for by a reduction in bias, i.e.  $|\overline{\mathbf{u}}_{\text{AWS}} - \overline{\mathbf{u}}_A|$  decreases. These ideas are discussed in greater detail in section 4. Note finally that the results for the Official versus ECMWF comparison in Fig. 5 largely mirror those of the ECMWF versus ACCESS comparison in Fig. 5, e.g. for the Darwin airport station and station group, Official outperforms ECMWF at the same times that ACCESS does, suggesting that either the Official forecast at these spatial scales is largely based on ACCESS, or that ECMWF is highly biased at these scales and times.

#### *b. Seasonal Comparison*

Figure 5 provides the climatological wind perturbation index values,  $\text{cwpi}$ , and confidence scores,  $P(\text{CWPI} > 0)$ , for the coastal station groups for  $\text{cwpi}_{\text{OA}}$ ,  $\text{cwpi}_{\text{OE}}$  and  $\text{cwpi}_{\text{EA}}$ , which represent the Official versus ACCESS, Official versus ECMWF, and ECMWF versus ACCESS comparisons, respectively. At the NT station group Official outperforms both ACCESS and ECMWF at 03:00 UTC with  $\text{cwpi}_{\text{OA}} = \text{cwpi}_{\text{OE}} = 0.4$ ,  $P(\text{cwpi}_{\text{OA}} > 0) = 94\%$  and  $P(\text{cwpi}_{\text{OE}} > 0) = 93\%$ . However, both ACCESS and ECMWF outperform Official at 23:00 and 00:00 UTC, consistent with the  $\overline{\text{wpi}}$  results in Fig. 2. The NT station group results are discussed in more detail in section 4.

At the North WA station group at 01:00, 03:00 and 04:00, Official outperforms ACCESS with confidence scores of 77, 78 and 90%, respectively; Official also outperforms ECMWF at 01:00 and 02:00 UTC with confidence scores above 99%. Figure 6 a) shows that ECMWF's poor performance at 01:00 and 02:00 UTC is simply due to its linear interpolation at these times, whereas

391 Official's outperformance of ACCESS at 01:00, 03:00 and 04:00 is due to ACCESS's climatolog-  
392 ical diurnal cycle being slightly out of phase with that of the AWS observations, and the Official  
393 forecast appearing to correct for this somewhat. Both Official and ECMWF slightly exaggerate  
394 the magnitude of the climatological sea-breeze with ACCESS doing a good job in this regard.

395 At the South WA station group from 01:00 to 05:00 UTC,  $cwpi_{OE}$  is positive with confidence  
396 scores of at least 88%, although  $cwpi_{OA}$  is negative or zero at these times. Figure 6 b) shows that  
397 ECMWF underestimates the westerly perturbations at these times, with these perturbations likely  
398 associated with boundary layer mixing processes, as discussed in section a. Each of Official,  
399 ACCESS and ECMWF underestimate the amplitude of the diurnal cycle between 02:00 and 10:00  
400 UTC, including both the westerly perturbations and the southerly sea-breeze perturbations.

401 At the NSW station group from 17:00 to 19:00 UTC,  $cwpi_{OA}$  and  $cwpi_{OE}$  are at least 0.4 and 0.1  
402 kn, respectively, with confidence scores of at least 95% and 75%, respectively. Figure 6 c) shows  
403 that these times correspond to a strange "dimple" in perturbation hodograph that is present in all  
404 four datasets. The Official hodograph closely resembles that of ACCESS, except for this dimple,  
405 which has been exaggerated relative to ACCESS. **Don't know what is going on here.** Figure 6 c)  
406 also shows that although ECMWF exaggerates the amplitude of the easterly sea-breeze perturba-  
407 tions, it captures the narrower shape of the AWS hodograph better than Official or ACCESS.

408 At the SA station group from 01:00 to 05:00 UTC and 09:00 to 11:00 UTC both  $cwpi_{OA}$  and  
409  $cwpi_{OE}$  are positive, with maximum values of 0.4 and 0.1 kn, although confidence scores do not  
410 exceed 88% and 65% respectively. Figure 6 shows that the Official forecast captures the amplitude  
411 of the perturbations from 01:00 to 05:00 UTC almost perfectly, matching the amplitude of the  
412 AWS perturbations better than both ACCESS and ECMWF. However, the Official diurnal cycle is  
413 slightly out of phase with the AWS cycle during this period, explaining why Official only slightly  
414 outperforms ACCESS in the results of Figures 5 a) and b).

415 While the cwpi values and confidence scores of Fig. 5 provide detailed information on which  
416 dataset’s climatological diurnal cycle best matches those of the AWS observations, cwpi on it’s  
417 own reveals little about the structure of the diurnal cycle, and provides little insight into forecast  
418 accuracy could be improved. Note that the hodographs in Fig. 6 are roughly elliptical in shape,  
419 suggesting that descriptive quantities can be estimated by fitting equations (5) and (6) to the zonal  
420 and meridional climatological perturbations, then calculating these quantities from the fit, as de-  
421 scribed in section 2.

422 Figure 8 provides the  $R^2$  values for the fits of the zonal and meridional perturbations to equations  
423 (5) and (6), respectively. The fit performs best at the coastal station group spatial scale, with  
424  $R^2$  generally above 95%. It also performs well at the airport station and airport station group  
425 scales, with a few exceptions, including the ACCESS and Official meridional perturbations at the  
426 Canberra airport station group, and the ECMWF zonal perturbations at Melbourne airport.

427 The ellipse fits are used to derive four descriptive quantities: amplitude (half the length of the  
428 semi-major axis), eccentricity, orientation (the angle the semi-major axis makes with lines of lati-  
429 tude) and the time of the peak in the diurnal cycle (the time at which the perturbations align with  
430 the semi-major axis, ignoring translational coefficients). Figure 9 provides these four quantities  
431 for each dataset and location across the three spatial scales. A variety of structural differences  
432 are apparent at a number of locations and scales. For example, Fig. 9 a) shows that at Brisbane  
433 airport, the amplitude of the AWS diurnal cycle is at least 1 kn greater than Official, ACCESS  
434 and ECMWF, and Fig. 9 c) shows that the orientation of the AWS diurnal cycle hodograph is at  
435 least 20 degrees (anti-clockwise) from the other datasets. Figures 10 a) and b) show hodographs of  
436 the Brisbane airport perturbation climatology and ellipse fit, respectively. Although the ellipse fit  
437 suppresses some of the asymmetric details, it captures the amplitudes and orientations of the real  
438 climatological diurnal cycles well. In this case the results show that the average AWS sea-breeze

approaches from the northeast, whereas the forecast and model sea-breezes approach more from the east-northeast. To check whether this just represents a direction bias of the Brisbane Airport station, Fig. 9 shows the climatological perturbations at the nearby Spitfire Channel station (see Fig. ?? for the location of this station, and other stations referred to in this section). While the amplitude bias is smaller at Spitfire Channel than Brisbane Airport, the directional bias is at least as high; a similar directional bias is evident at the nearby Inner Beacon station, although the bias is smaller than at Spitfire Channel and Brisbane Airport. Thus, the directional bias in Official, ACCESS and ECMWF at these stations is likely genuine, and not just a consequence of biased AWS observations. Figure 1 x) shows there are two small islands to the east of Brisbane airport; the more northwesterly orientation of the Brisbane Airport sea-breeze suggests these islands may be channelling winds between the east coast of Brisbane and the west coasts of these islands, and that this local effect is not being captured in Official, ACCESS or ECMWF.

Another example is the Hobart Airport station. Figure 9 c) shows that the ellipse fits for the AWS perturbations are oriented 31, 35 and 62 degrees anti-clockwise from the ECMWF, Official and ACCESS ellipse fits, respectively. Figures 8 a) and b) show that the ellipse fit for the AWS perturbations at Hobart airport only achieve  $R^2$  values of 59% and 68% for the  $u$  and  $v$  components, respectively, although figures 10 d) and e) show that the fit still captures the orientation accurately; the deficiency is more with the amplitude of the AWS diurnal cycle. Figure 8 c) shows the climatological perturbations at the Hobart (city) station, which also show a large difference in orientation between ACCESS and AWS. Given the timing of the westerly perturbations in ACCESS, and the fact that the prevailing winds around Tasmania are Hobart, these results suggest that ACCESS is exaggerating the boundary layer mixing processes involved in the diurnal cycle, whereas ECMWF better captures the southerly sea-breeze component of the cycle.

462 The South WA station group also provides an interesting example. Here the ACCESS and  
463 Official ellipse fits are oriented at least 49 degrees anti-clockwise from those of AWS and ECMWF,  
464 and the time of the peak in the diurnal cycles of ACCESS and Official is at least 4.3 hours earlier  
465 than AWS and ECMWF. This occurs because eccentricity values are low for this station group,  
466 and Figure 6 b) shows that the westerly perturbations associated with boundary layer mixing are  
467 slightly faster than the corresponding southerly sea-breeze perturbations, which peak later, for  
468 both ACCESS and Official, but slightly slower for ECMWF and Official. A similar issue affects  
469 the VIC station group, explaining why the AWS ellipse fit is oriented at least 49 degrees anti-  
470 clockwise from those of the other datasets.

471 Finally, figure 9 suggests that at the Darwin Airport, Darwin Airport station group, and NT sta-  
472 tion group, the AWS wind perturbations align with the semi-major axis after those of the other  
473 datasets, and in the case of the NT station group alignment occurs at least 2.3 hours later; fur-  
474 thermore, the amplitude of the Official ellipse fit is in each case higher than those of the other  
475 datasets. “Alignment” is probably the wrong word here. Figure 11 shows that these biases are  
476 indeed evident in the perturbation climatologies themselves, with the exception of the Darwin  
477 Airport amplitude bias, where the asymmetric hodograph shapes lead to the ellipse fit underesti-  
478 mating the amplitude of the AWS diurnal cycle Needs to be clarified to better distinguish between  
479 “ellipse” amplitude and diurnal cycle amplitude. Furthermore, should we interpret the NT station  
480 group results as genuine evidence of a timing bias?

#### 481 4. Discussion

482 The two most important results of section 3 to explain are, first, why equations 5 and 6 provide  
483 such a good fit to the climatological perturbations and, second, why there are such substantial  
484 changes in the performance of the Official forecast at the different spatial and temporal scales.

The idea that diurnal wind cycles can be described by ellipses originated with Haurwitz (1947).

Haurwitz obtained exact solutions for  $u$  and  $v$  resembling equations (3) and (4) for the simple model

$$\frac{du}{dt} - fv + ku = F_x - F(t) \quad (9)$$

$$\frac{dv}{dt} + fu + kv = F_y \quad (10)$$

where  $u, v$  are taken in a coordinate system where the  $u$  axis is normal to the coast,  $f$  is the Coriolis parameter,  $k$  is a linear friction coefficient,  $(F_x, F_y)$  represents a constant synoptic scale pressure gradient force,  $\omega$  is the angular frequency of earth's rotation, and

$$F(t) = \frac{A}{\pi} + \frac{A}{2} \cos(\omega t) \quad (11)$$

is the pressure gradient force normal to the coastline induced by the diurnally varying air temperature contrast over the land and sea surfaces. Kusuda and Alpert (1983) extended this model slightly, but the fundamentals are the same. The limitations of this model are discussed extensively by Haurwitz (1947) and Kusuda and Alpert (1983), but the most important given the results of section 3 involve the choice of  $F(t)$ , which does not sufficiently capture the asymmetries in daytime heating and nighttime cooling, and the fact that the model has no vertical dimension, and therefore cannot capture the boundary layer mixing processes that in many cases play a significant role in the diurnal wind cycle. This might work better in the introduction or methods sections - there's not actually very much to discuss!

I tried modifying the pressure perturbation terms  $\frac{A}{\pi} + \frac{A}{2} \cos(\omega t)$  so that the new ellipse fit of equations (5) and (6) become solutions to equations (9) and (10), but with no luck. For example, simply changing to  $F(t)$  to  $\frac{A}{\pi} + \frac{A}{2} \cos(\alpha(\psi, t))$  doesn't work, nor does expanding this expression as a Fourier series and solving each term individually.

The second result of section 3 that requires explanation are the differences in the performance of the Official forecast at the different spatial and temporal scales. Consider first just the zonal components of the AWS and Official wind perturbations, denoted by  $u_{\text{AWS}}$  and  $u_{\text{O}}$  respectively. Considering just the values at a particular hour UTC, at a particular station, over the entire June, July, August time period, the mean square error  $\text{mse}(u_{\text{AWS}}, u_{\text{O}}) = \overline{(u_{\text{AWS}} - u_{\text{O}})^2}$  can be decomposed

$$\text{mse}(u_{\text{AWS}}, u_{\text{O}}) = \underbrace{\text{var}(u_{\text{AWS}}) + \text{var}(u_{\text{O}}) - 2 \cdot \text{covar}(u_{\text{AWS}}, u_{\text{O}})}_{\text{var}(u_{\text{AWS}} - u_{\text{O}})} + \underbrace{(\bar{u}_{\text{AWS}} - \bar{u}_{\text{O}})^2}_{\text{bias}^2} \quad (12)$$

where  $\text{var}$ ,  $\text{covar}$  and over-bars denote the sample variance, covariance and mean respectively. The first three terms are the total variance of  $u_{\text{AWS}} - u_{\text{O}}$ , whereas the last term is the square of the bias between  $u_{\text{AWS}}$  and  $u_{\text{O}}$ . This decomposition can also be applied to wind perturbations that have first been spatially averaged over a station group, and to  $\text{mse}(u_{\text{AWS}}, u_{\text{E}})$  and  $\text{mse}(u_{\text{AWS}}, u_{\text{A}})$ , where  $u_{\text{E}}$  and  $u_{\text{A}}$  are the ECMWF and ACCESS zonal perturbations, respectively.

Figure 12 shows each term in the mean square error decomposition of equation 12 for both  $\text{mse}(u_{\text{AWS}}, u_{\text{O}})$  and  $\text{mse}(u_{\text{AWS}}, u_{\text{E}})$ , for Darwin Airport, the Darwin station group, and the NT station group. At Darwin Airport,  $\text{mse}(u_{\text{AWS}}, u_{\text{O}})$  exceeds  $\text{mse}(u_{\text{AWS}}, u_{\text{E}})$  from 04:00 to 16:00 UTC due to higher total variance, whereas outside of these times  $\text{mse}(u_{\text{AWS}}, u_{\text{E}})$  exceeds  $\text{mse}(u_{\text{AWS}}, u_{\text{O}})$  due to larger bias. The higher total variance of  $u_{\text{AWS}} - u_{\text{O}}$  occurs because  $\text{var}(u_{\text{O}}) > \text{var}(u_{\text{E}})$ , with this additional variability mostly random from 04:00 to 14:00 UTC, i.e.  $u_{\text{O}}$  is not sufficiently correlated with  $u_{\text{AWS}}$  at these times for the additional variability of  $u_{\text{O}}$  to produce a reduction in mean square error. Thus, while the bias between Official and AWS is lower, or about the same, as that between ECMWF and AWS, the higher random variability of Official results in higher mean square error for most of the day. Figure 13 shows similar conclusions can be drawn for the meridional perturbations at Darwin Airport, although in this case  $\text{var}(u_{\text{O}}) > \text{var}(u_{\text{E}})$  for the entire day. Most



526 of the difference between the WPI and CWPI scores for the Official versus ECMWF comparison  
527 at Darwin Airport in Figures 5 and 7, respectively, can be explained through the different mean  
528 square error and bias terms for the zonal perturbations alone. Figure 11 a) shows that ECMWF's  
529 climatological perturbations underestimate the easterly perturbations from 00:00 to 03:00 UTC,  
530 which are presumably associated with boundary layer mixing processes. Official does a better job  
531 of resolving these easterly perturbations, but is generally outperformed by ECMWF in resolving  
532 the northerly sea-breeze perturbations. Similar points can be made for the Darwin and NT coastal  
533 station groups. While spatial averaging reduces a portion of the unpredictable variability in Offi-  
534 cial, Official also often has larger meridional biases at these scales compared to ECMWF. Figures  
535 11 and 9 show that these biases can be explained in terms of amplitude and orientation differences  
536 between Official, ECMWF and AWS.

537 These examples illustrate the idea that the additional unpredictable variability introduced by a  
538 higher resolution edited forecast needs to be “paid for” by a reduction in bias, otherwise the net re-  
539 sult will just be an increase in error. However, although a high resolution edited forecast may have  
540 higher mean squared error compared with observations than an unedited low resolution model, the  
541 former may capture variability more realistically, and hence better represent the possibility of ex-  
542 tremes, even if the timing of these extremes is unpredictable; which of the two constitutes a better  
543 forecast therefore depends entirely on the application. For instance, in engineering applications,  
544 the possibility of wind extremes of a certain magnitude may be most important, regardless of when  
545 they occur, whereas in aviation or sailing it may be more important to minimise the mean square  
546 error. This is obviously speculation as I know little about either of these applications. I hope there  
547 are more appropriate examples. The fact that high and low resolution model guidance products are  
548 used at different times, and on different days, implies that the Official forecast is inconsistent in

549 which measures of accuracy it intends to maximise, and more thought therefore needs to be given  
550 to this issue.

## 551 **5. Conclusion**

552 We have

## 553 **References**

554 Brown, A. L., C. L. Vincent, T. P. Lane, E. Short, and H. Nguyen, 2017: Scatterometer estimates  
555 of the tropical sea-breeze circulation near Darwin, with comparison to regional models. *Quart.*  
556 *J. Roy. Meteor. Soc.*, doi:10.1002/qj.3131.

557 Bureau of Meteorology, 2010: Operational implementation of the ACCESS numerical weather  
558 prediction systems. Tech. rep., Bureau of Meteorology, Melbourne, Victoria. [Available online  
559 at <http://www.bom.gov.au/australia/charts/bulletins/apob83.pdf>].

560 Ebert, E. E., 2008: Fuzzy verification of high-resolution gridded forecasts: a review and proposed  
561 framework. *Meteor. Appl.*, **15** (1), 51–64, doi:10.1002/met.25, URL [https://rmets.onlinelibrary.](https://rmets.onlinelibrary.wiley.com/doi/abs/10.1002/met.25)  
562 [wiley.com/doi/abs/10.1002/met.25](https://rmets.onlinelibrary.wiley.com/doi/pdf/10.1002/met.25), [https://rmets.onlinelibrary.wiley.com/doi/pdf/10.1002/met.](https://rmets.onlinelibrary.wiley.com/doi/pdf/10.1002/met.25)  
563 25.

564 Efron, B., 1979: Bootstrap methods: Another look at the jackknife. *The Annals of Statistics*, **7** (1),  
565 1–26, doi:10.1214/aos/1176344552.

566 European Center for Medium Range Weather Forecasting, 2018: *Part IV : Physical processes*.  
567 No. 4, IFS Documentation, European Center for Medium Range Weather Forecasting, [Avail-  
568 able online at <https://www.ecmwf.int/node/18714>].

569 Gille, S. T., S. G. Llewellyn Smith, and N. M. Statom, 2005: Global observations of the  
570 land breeze. *Geophysical Research Letters*, **32** (5), doi:10.1029/2004GL022139, URL <https://agupubs.onlinelibrary.wiley.com/doi/abs/10.1029/2004GL022139>.  
571

572 Haurwitz, B., 1947: Comments on the sea-breeze circulation. *Journal of Meteorol-*  
573 *ogy*, **4** (1), 1–8, doi:10.1175/1520-0469(1947)004<0001:COTSBC>2.0.CO;2, URL  
574 [https://doi.org/10.1175/1520-0469\(1947\)004<0001:COTSBC>2.0.CO;2](https://doi.org/10.1175/1520-0469(1947)004<0001:COTSBC>2.0.CO;2),  
575 [https://doi.org/10.1175/1520-0469\(1947\)004<0001:COTSBC>2.0.CO;2](https://doi.org/10.1175/1520-0469(1947)004<0001:COTSBC>2.0.CO;2).

576 Kusuda, M., and P. Alpert, 1983: Anti-clockwise rotation of the wind hodograph.  
577 part i: Theoretical study. *Journal of the Atmospheric Sciences*, **40** (2), 487–499,  
578 doi:10.1175/1520-0469(1983)040<0487:ACROTW>2.0.CO;2, URL [https://doi.org/10.1175/](https://doi.org/10.1175/1520-0469(1983)040<0487:ACROTW>2.0.CO;2)  
579 [1520-0469\(1983\)040<0487:ACROTW>2.0.CO;2](https://doi.org/10.1175/1520-0469(1983)040<0487:ACROTW>2.0.CO;2).

580 Lock, A. P., A. R. Brown, M. R. Bush, G. M. Martin, and R. N. B. Smith, 2000: A new bound-  
581 ary layer mixing scheme. part i: Scheme description and single-column model tests. *Monthly*  
582 *Weather Review*, **128** (9), 3187–3199, doi:10.1175/1520-0493(2000)128<3187:ANBLMS>2.  
583 0.CO;2, URL [https://doi.org/10.1175/1520-0493\(2000\)128<3187:ANBLMS>2.0.CO;2](https://doi.org/10.1175/1520-0493(2000)128<3187:ANBLMS>2.0.CO;2), [https://doi.org/10.1175/1520-0493\(2000\)128<3187:ANBLMS>2.0.CO;2](https://doi.org/10.1175/1520-0493(2000)128<3187:ANBLMS>2.0.CO;2).  
584

585 Louis, J.-F., 1979: A parametric model of vertical eddy fluxes in the atmosphere. *Boundary-*  
586 *Layer Meteorology*, **17** (2), 187–202, doi:10.1007/BF00117978, URL [https://doi.org/10.1007/](https://doi.org/10.1007/BF00117978)  
587 [BF00117978](https://doi.org/10.1007/BF00117978).

588 Lynch, K. J., D. J. Brayshaw, and A. Charlton-Perez, 2014: Verification of european sub-  
589 seasonal wind speed forecasts. *Monthly Weather Review*, **142** (8), 2978–2990, doi:10.1175/  
590 MWR-D-13-00341.1, URL <https://doi.org/10.1175/MWR-D-13-00341.1>, <https://doi.org/10.1175/MWR-D-13-00341.1>.  
591

592 Pinson, P., and R. Hagedorn, 2012: Verification of the ecmwf ensemble forecasts of wind  
593 speed against analyses and observations. *Meteor. Appl.*, **19** (4), 484–500, doi:10.1002/  
594 met.283, URL <https://rmets.onlinelibrary.wiley.com/doi/abs/10.1002/met.283>, <https://rmets.onlinelibrary.wiley.com/doi/pdf/10.1002/met.283>.  
595

596 Smith, J. C., R. Thresher, R. Zavadil, E. DeMeo, R. Piwko, B. Ernst, and T. Ackermann, 2009: A  
597 mighty wind. *IEEE Power and Energy Magazine*, **7** (2), 41–51, doi:10.1109/MPE.2008.931492.

598 Wilks, D. S., 2011: *Statistical methods in the atmospheric sciences. [electronic resource]*. Inter-  
599 national geophysics series: v. 100, Elsevier.

600 Zwiers, F. W., and H. von Storch, 1995: Taking serial correlation into account in tests of the mean.  
601 *Journal of Climate*, **8** (2), 336–351, doi:10.1175/1520-0442(1995)008<0336:TSCIAI>2.0.CO;2,  
602 URL [https://doi.org/10.1175/1520-0442\(1995\)008<0336:TSCIAI>2.0.CO;2](https://doi.org/10.1175/1520-0442(1995)008<0336:TSCIAI>2.0.CO;2), [https://doi.org/10.1175/1520-0442\(1995\)008<0336:TSCIAI>2.0.CO;2](https://doi.org/10.1175/1520-0442(1995)008<0336:TSCIAI>2.0.CO;2).  
603

|     |   |    |
|-----|---|----|
| 604 | <b>LIST OF FIGURES</b>  |    |
| 605 | <b>Fig. 1.</b> Locations of the automatic weather stations used in this study. Stars indicate capital city                            |    |
| 606 | airport stations. Height and depth shading intervals every 200 and 1000 m, respectively. . . . .                                      | 30 |
| 607 | <b>Fig. 2.</b> Heatmaps of $\overline{WPI}$ values and confidence scores for each coastal station group and hour of                   |    |
| 608 | the day: a) and b), Official versus ACCESS, c) and d) Official versus ECMWF, e) and f)  |    |
| 609 | ECMWF versus ACCESS. Positive $\overline{WPI}$ values mean that the former dataset in each pair                                       |    |
| 610 | is on average closer to observations than the latter dataset. Confidence scores provide the   |    |
| 611 | probability the population $\overline{WPI}$ is greater than zero. Values within the heatmaps are accurate                             |    |
| 612 | to two significant figures. . . . .   | 31 |
| 613 | <b>Fig. 3.</b> Time series, a) and b), of $\overline{wpi}_{OA}$ and $\overline{wpi}_{OE}$ for, a), the NT station group at 23:00 UTC, |    |
| 614 | and b), the south WA station group at 05:00 UTC. Hodographs, c) to f), showing change in  |    |
| 615 | winds, c) and e), and wind perturbations, d) and f), for the NT station group, c) and d), and   |    |
| 616 | south WA station group, e) and f). . . . .  | 32 |
| 617 | <b>Fig. 4.</b> Hodographs showing change in winds with height at, a), Darwin Airport, and b), Perth                                   |    |
| 618 | Airport. . . . .  | 33 |
| 619 | <b>Fig. 5.</b> The $\overline{wpi}_{OE}$ (Official versus ECMWF comparison) values, a) and c), and confidence scores,                 |    |
| 620 | b) and d), for the airport stations, a) and b), and airport station groups, c) and d), respectively. . . . .                          | 34 |
| 621 | <b>Fig. 6.</b> Climatological hodographs. . . . .   | 37 |
| 622 | <b>Fig. 7.</b> As in Fig. 5, but for the $cwpi$ values and confidence scores. . . . .   | 38 |
| 623 | <b>Fig. 8.</b> Could also provide an analogous figure showing the use of the function $\alpha$ provides a signifi-                    |    |
| 624 | cant improvement over the basic ellipse fit - or instead just quote some numbers? Or maybe  |    |
| 625 | these figures are entirely unnecessary? . . . . .   | 39 |
| 626 | <b>Fig. 9.</b> Ellipse fits. If we were to include any analysis for alternative time periods (e.g. summer                             |    |
| 627 | 2017/18 for contrast; or could do 18/19 if I were to go back to BoM to get the data) a copy   |    |
| 628 | of this figure could be a good choice. Could explain changes in diurnal cycle properties, e.g.  |    |
| 629 | amplitude, with seasonal changes to background winds, heating, etc. Note some issues with   |    |
| 630 | timing and amplitude values due to asymmetry - could instead just show eccentricity and   |    |
| 631 | orientation values? . . . . .   | 40 |
| 632 | <b>Fig. 10.</b> Ellipse fits. Could instead just provide one example. . . . .   | 41 |
| 633 | <b>Fig. 11.</b> Ellipse fits. Could also include the ellipses, but this makes the figure very large. . . . .                          | 42 |
| 634 | <b>Fig. 12.</b> Actual perturbation standard deviation values. Note that official performs the worst at this                          |    |
| 635 | scale! . . . . .  | 43 |
| 636 | <b>Fig. 13.</b> Actual perturbation standard deviation values. Note that official performs the worst at this                          |    |
| 637 | scale! . . . . .  | 44 |

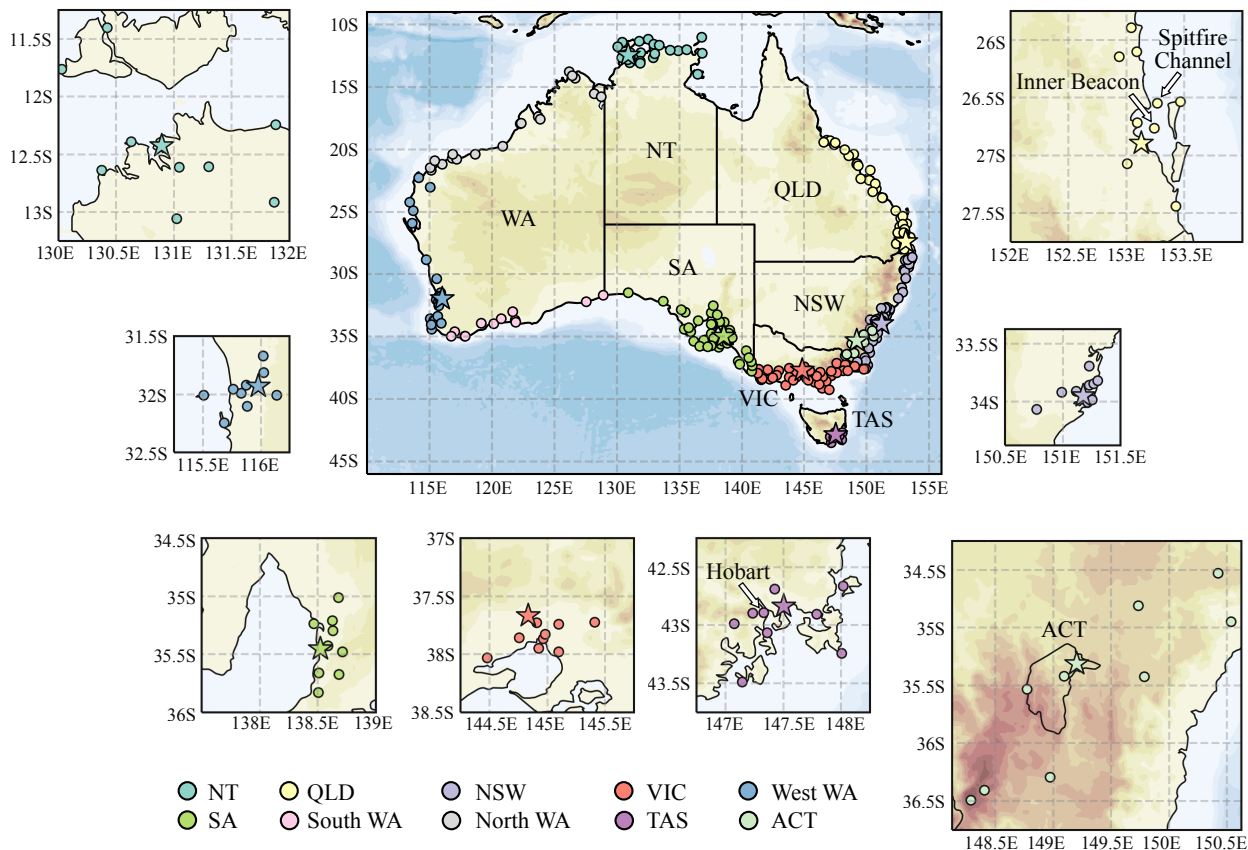


FIG. 1. Locations of the automatic weather stations used in this study. Stars indicate capital city airport stations. Height and depth shading intervals every 200 and 1000 m, respectively.

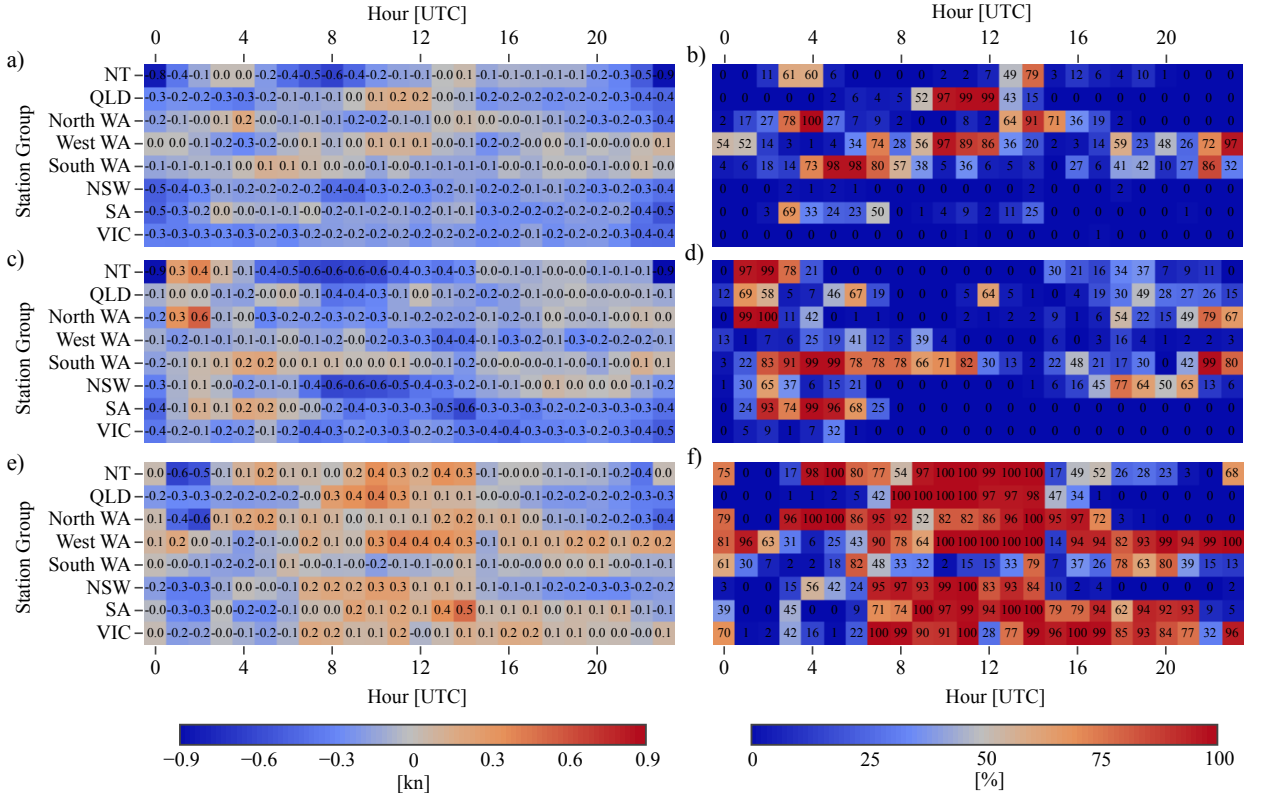


FIG. 2. Heatmaps of  $\overline{\text{WPI}}$  values and confidence scores for each coastal station group and hour of the day: a) and b), Official versus ACCESS, c) and d) Official versus ECMWF, e) and f) ECMWF versus ACCESS. Positive  $\overline{\text{WPI}}$  values mean that the former dataset in each pair is on average closer to observations than the latter dataset. Confidence scores provide the probability the population  $\overline{\text{WPI}}$  is greater than zero. Values within the heatmaps are accurate to two significant figures.

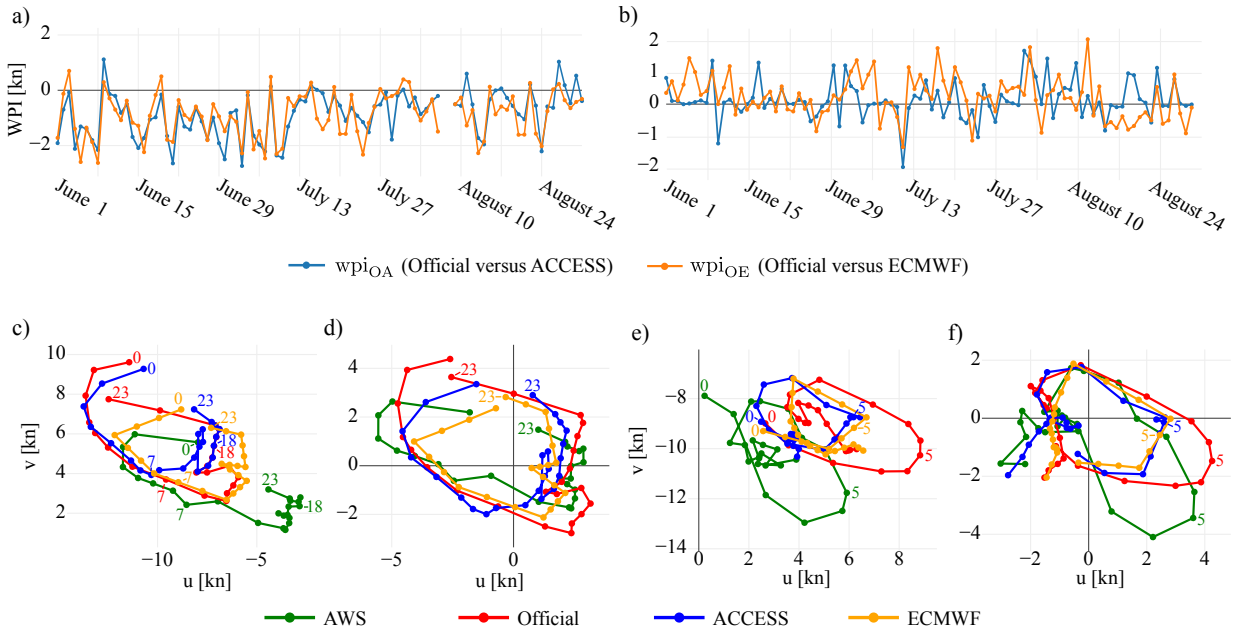


FIG. 3. Time series, a) and b), of  $\overline{wpi}_{OA}$  and  $\overline{wpi}_{OE}$  for, a), the NT station group at 23:00 UTC, and b), the south WA station group at 05:00 UTC. Hodographs, c) to f), showing change in winds, c) and e), and wind perturbations, d) and f), for the NT station group, c) and d), and south WA station group, e) and f).



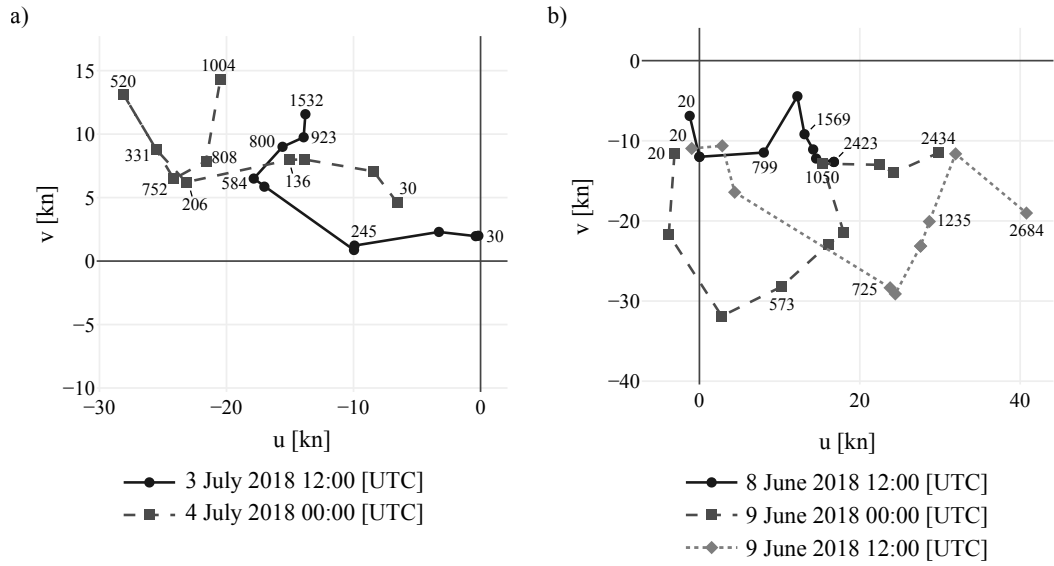


FIG. 4. Hodographs showing change in winds with height at, a), Darwin Airport, and b), Perth Airport.

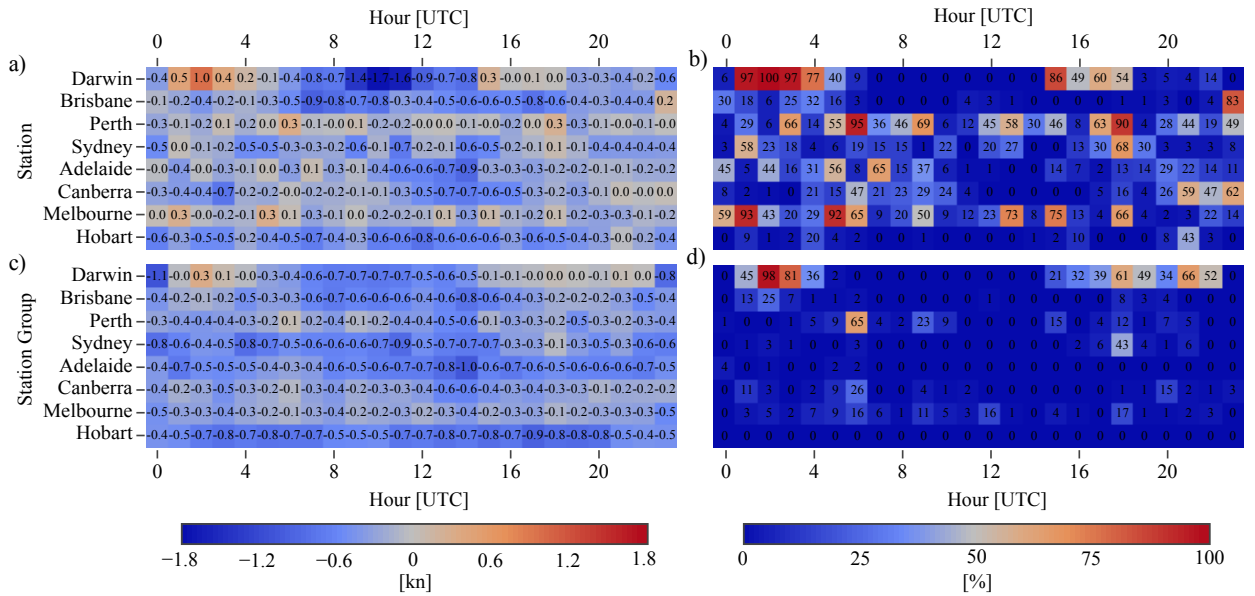
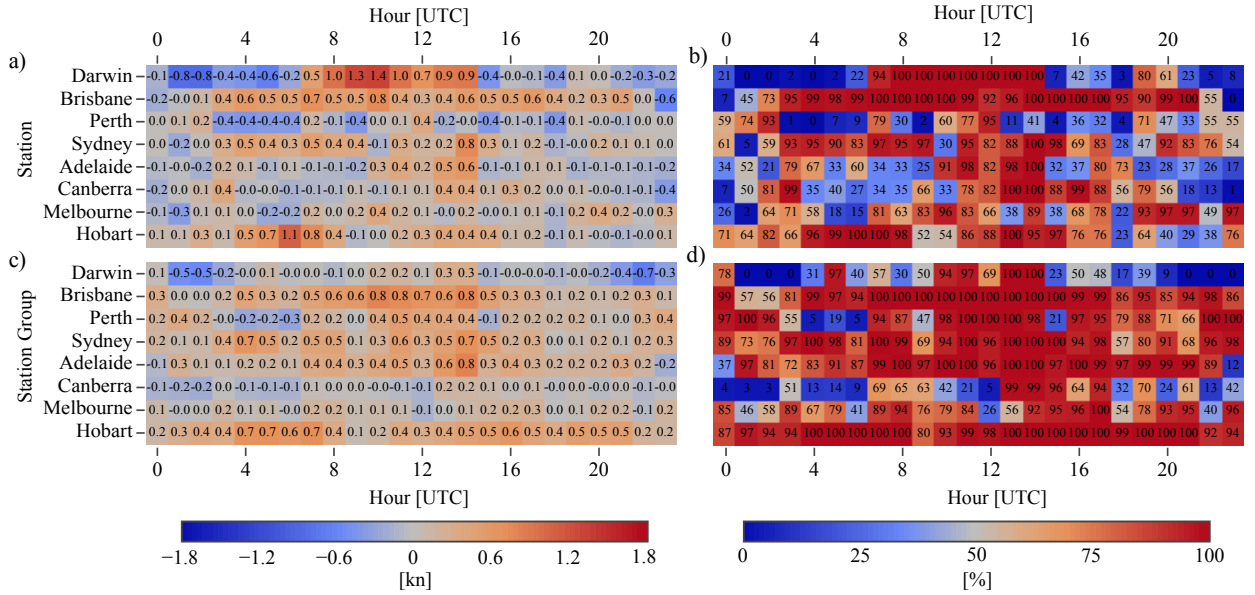
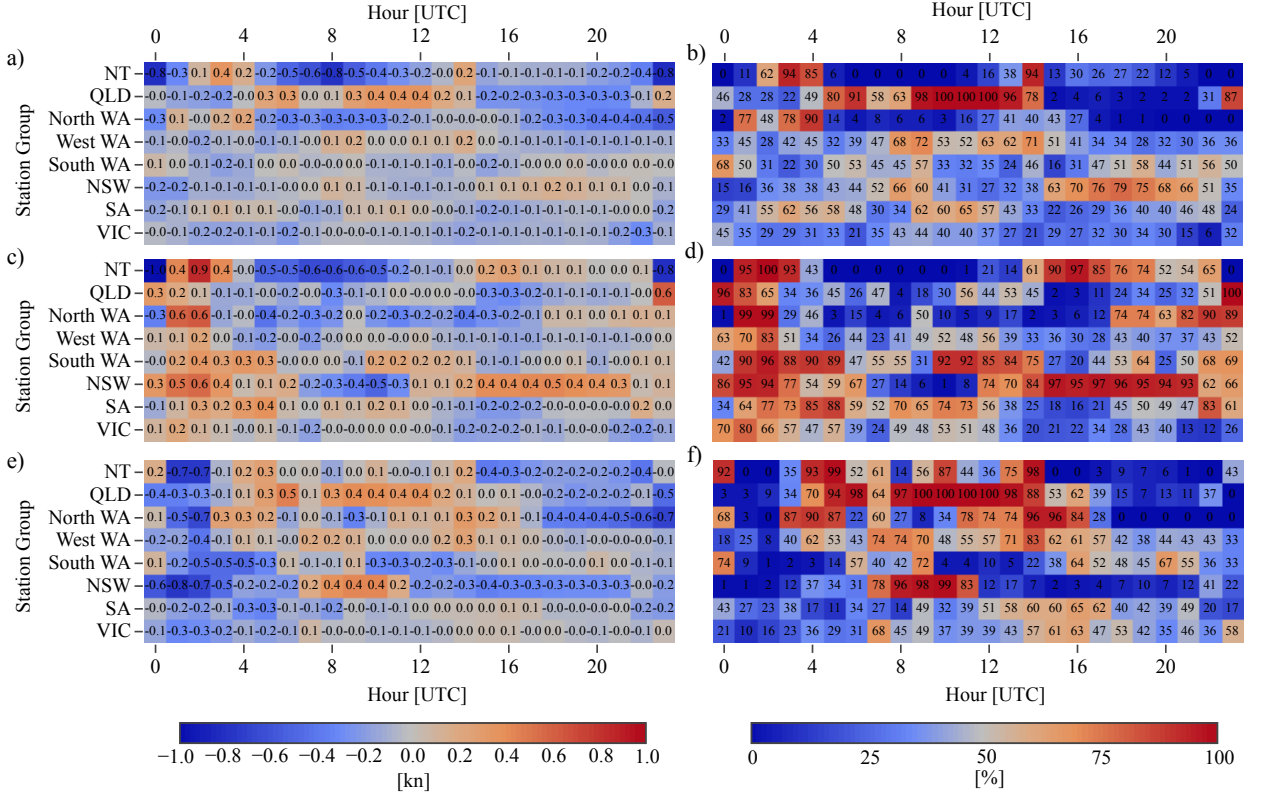


FIG. 5. The  $\overline{wpi}_{OE}$  (Official versus ECMWF comparison) values, a) and c), and confidence scores, b) and d), for the airport stations, a) and b), and airport station groups, c) and d), respectively.





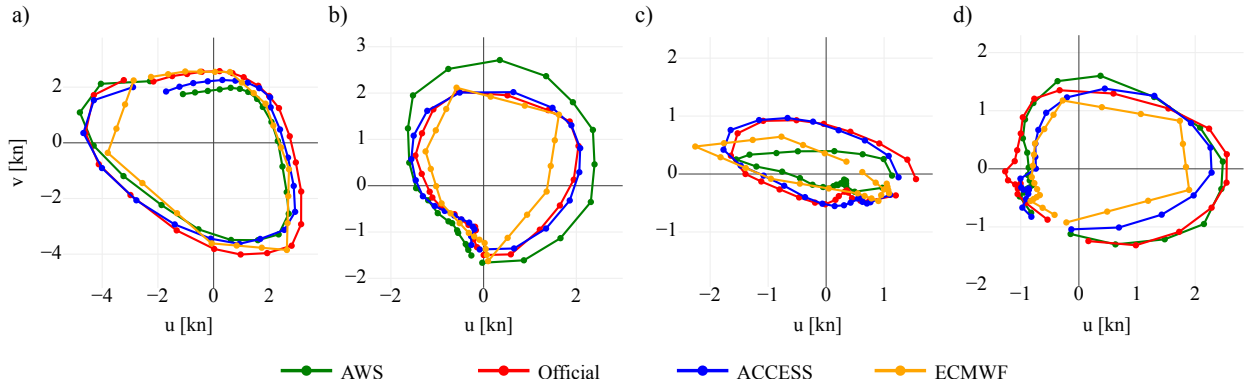


FIG. 6. Climatological hodographs.

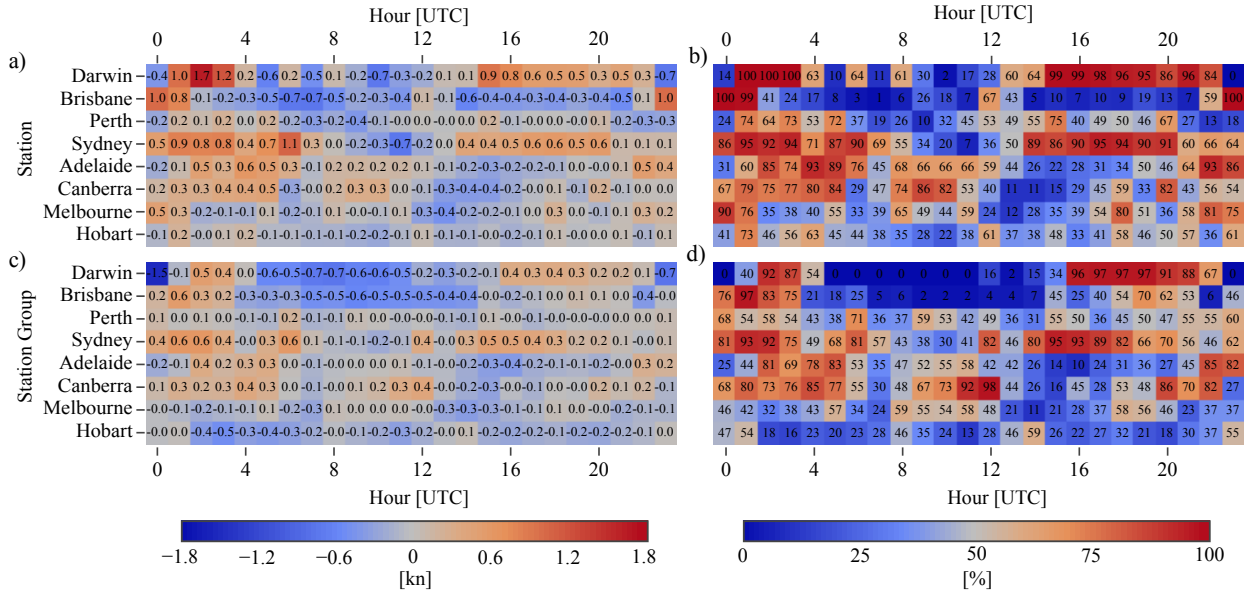


FIG. 7. As in Fig. 5, but for the cwpi values and confidence scores.

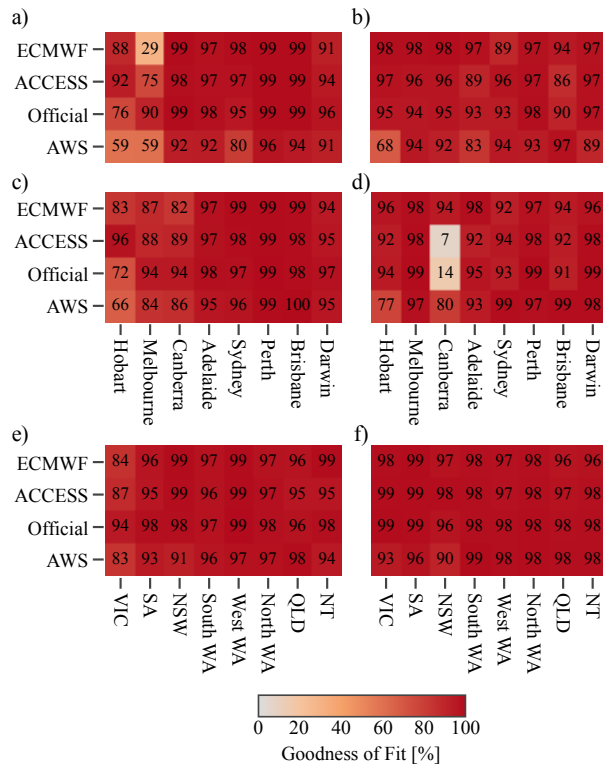


FIG. 8. Could also provide an analogous figure showing the use of the function  $\alpha$  provides a significant improvement over the basic ellipse fit - or instead just quote some numbers? Or maybe these figures are entirely unnecessary?

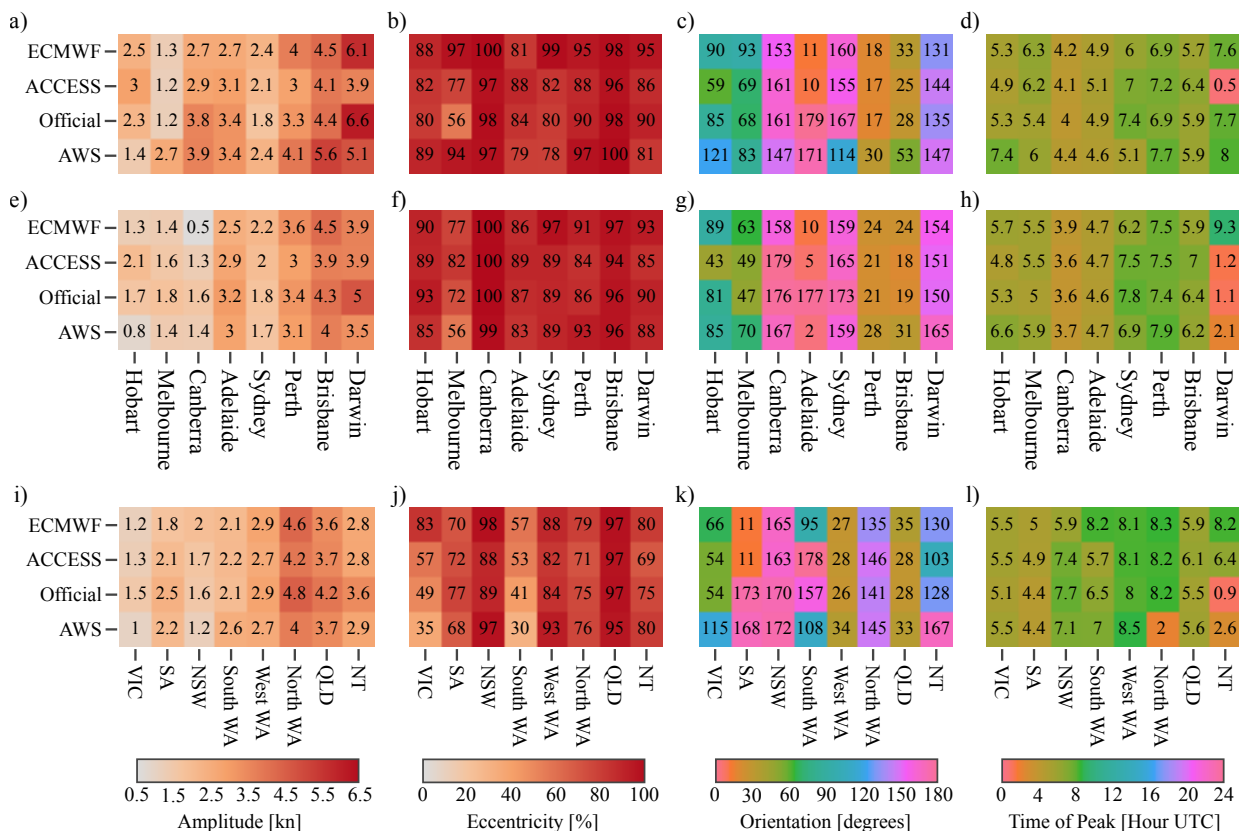


FIG. 9. Ellipse fits. If we were to include any analysis for alternative time periods (e.g. summer 2017/18 for contrast; or could do 18/19 if I were to go back to BoM to get the data) a copy of this figure could be a good choice. Could explain changes in diurnal cycle properties, e.g. amplitude, with seasonal changes to background winds, heating, etc. Note some issues with timing and amplitude values due to asymmetry - could instead just show eccentricity and orientation values?



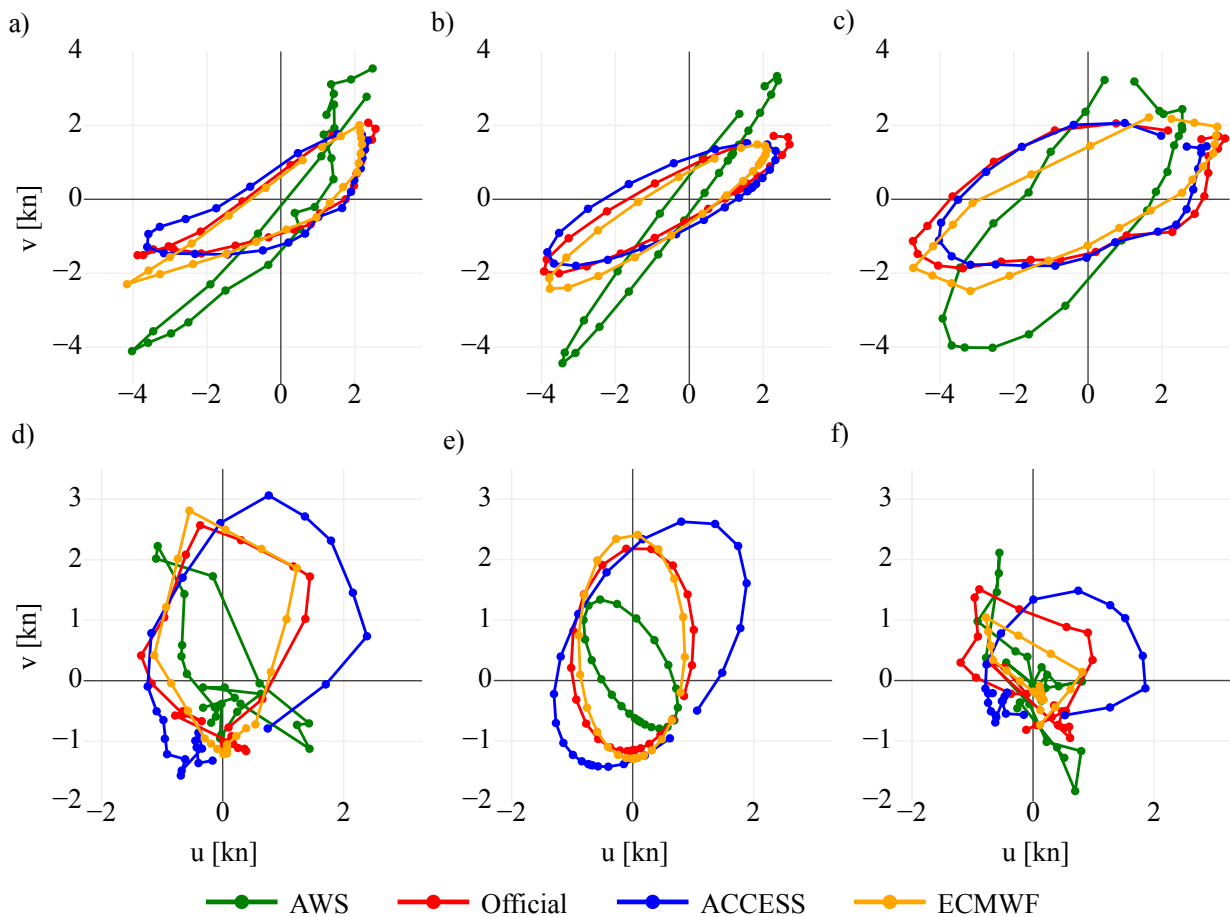


FIG. 10. Ellipse fits. Could instead just provide one example.

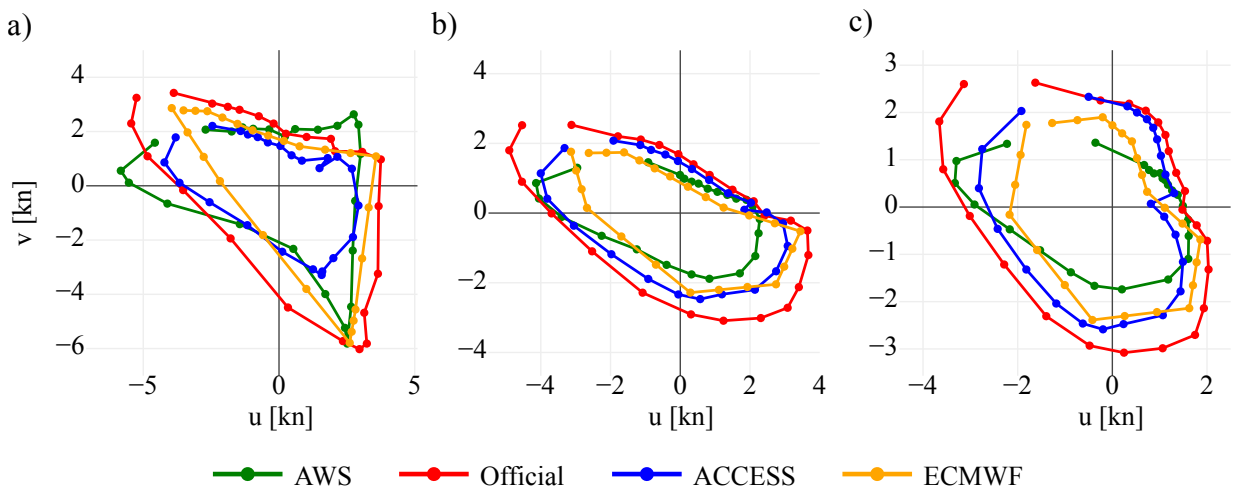


FIG. 11. Ellipse fits. Could also include the ellipses, but this makes the figure very large.

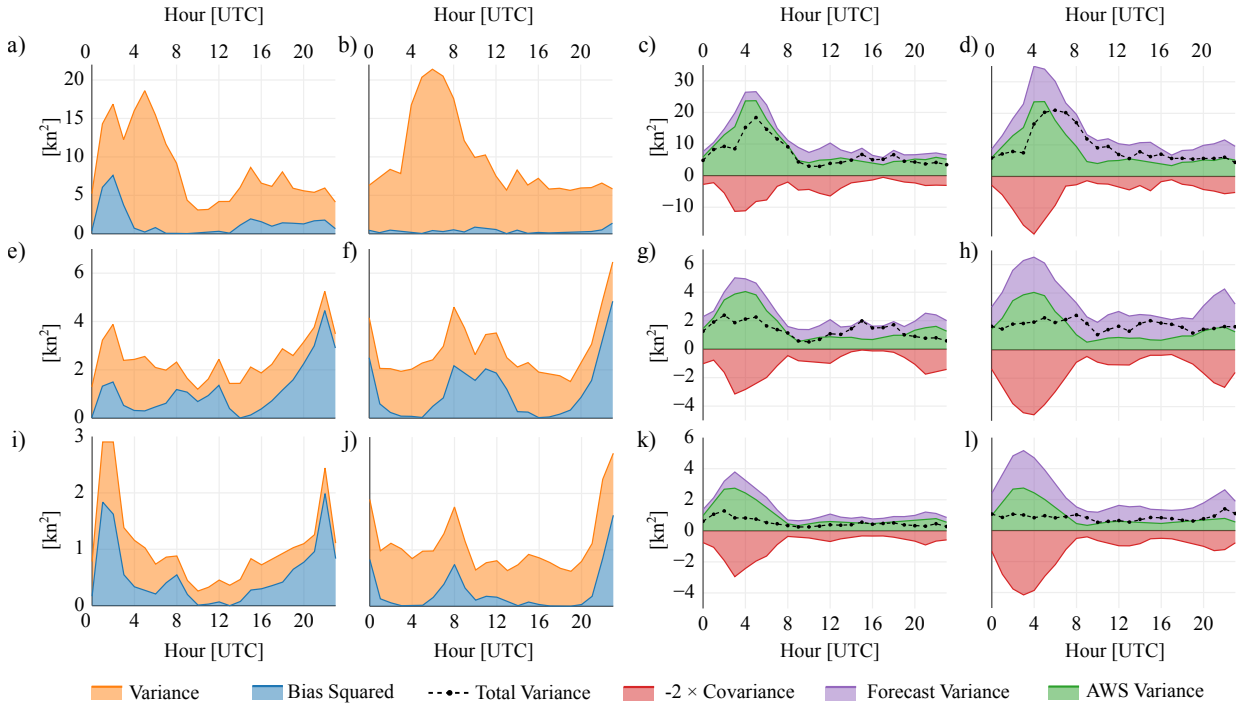


FIG. 12. Actual perturbation standard deviation values. Note that official performs the worst at this scale!

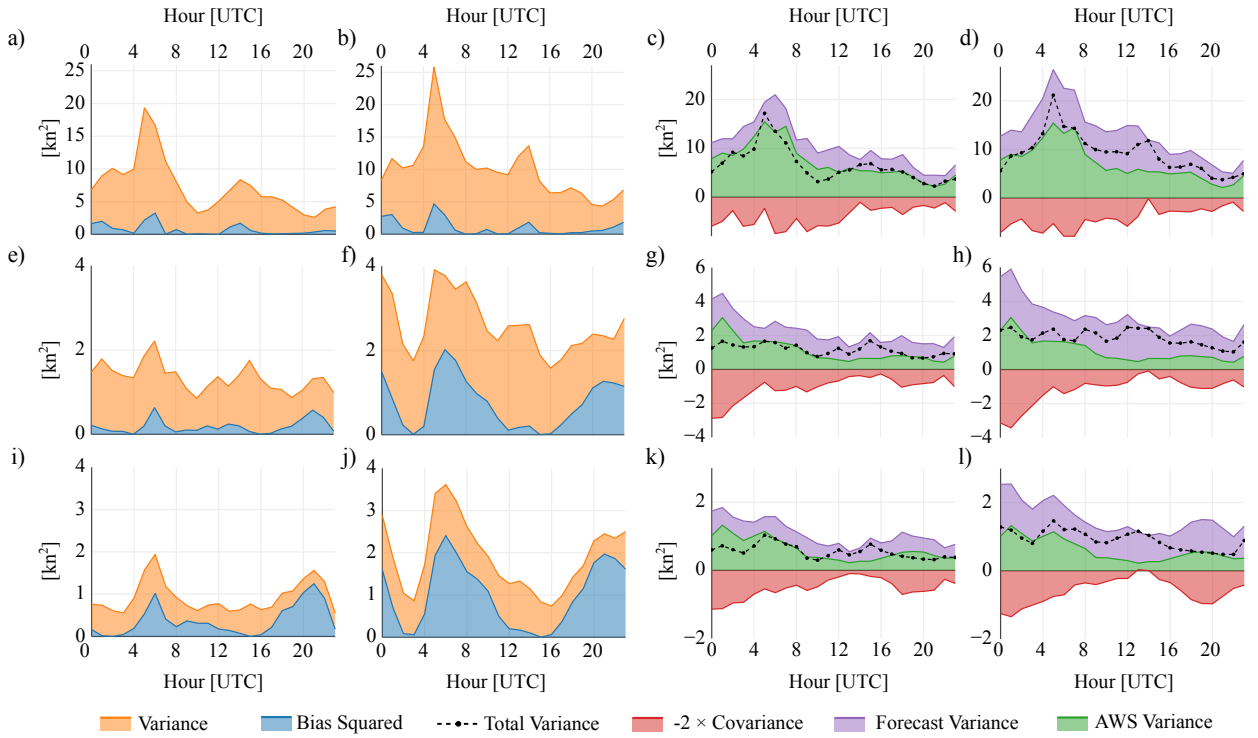


FIG. 13. Actual perturbation standard deviation values. Note that official performs the worst at this scale!